Electromagnons in multiferroic manganites



2008 J. Phys.: Condens. Matter 20 434209

(http://iopscience.iop.org/0953-8984/20/43/434209)

J. Phys.: Condens. Matter **20** (2008) 434209 (10pp) doi:10.1088/0953-8984/20/43/434209

# Electromagnons in multiferroic manganites

**A Pimenov[1], A M Shuvaev[1], A A Mukhin[2] and A Loidl[3]**

[1] Experimentelle Physik 4, Universität Würzburg, D-97074 Würzburg, Germany
[2] General Physics Institute, Russian Academy of Sciences, 119991 Moscow, Russia
[3] EP V, Center for Electronic Correlations and Magnetism, Universität Augsburg, D-86135 Augsburg, Germany

Received 11 March 2008, in final form 20 May 2008
Published 9 October 2008
Online at stacks.iop.org/JPhysCM/20/434209

**Abstract**

We review terahertz experiments on magnetoelectric excitations in rare earth multiferroic manganites $RMnO_3$ with R = Gd, Tb, Dy, (Eu:Y). In all these compounds characteristic excitations of the novel type, called electromagnons, have been observed for frequencies $10\ cm^{-1} < \nu < 30\ cm^{-1}$. From the spectroscopic point of view electromagnons are responsible for the magnetoelectric effects in $RMnO_3$ and, contrary to magnons, are excited only by electric components of the electromagnetic wave. In all compositions the electromagnons appear as a broad Debye-like contribution in the sinusoidally modulated antiferromagnetic phase and transform to well-defined excitations as the magnetic structure becomes spiral. At the lowest temperatures the fine structure of electromagnons is observed, reflecting the increasing complexity of the magnetic structure.

(Some figures in this article are in colour only in the electronic version)

## 1. Introduction

Most interactions in solid state physics are accompanied by appropriate elementary excitations which can be investigated using spectroscopic methods. Such excitations are generally observed at frequencies corresponding to the characteristic energy scale of the interaction. Prominent examples of this correspondence are elastic interactions (phonons) and magnetic interactions (magnons). Including additional interactions do not automatically lead to new excitations in the spectra. If the new interaction is weak, it leads simply to a renormalization of existing excitation frequencies. This seems not to be the case for multiferroic manganites $RMnO_3$ with modulated magnetic structures, where the magnetoelectric (ME) interaction is strong due to the improper character of the ferroelectricity. Assuming the static dielectric constant as a measure of the magnetoelectricity, the changes in magnetic fields in some cases may even exceed 100% [1]. Therefore, the appearance of excitations of new type can be expected in these compounds.

Experimentally, the first observation of coupled magnetoelectric excitations in $GdMnO_3$ and $TbMnO_3$ were reported by Pimenov *et al* [2], who introduced the nomenclature 'electromagnons': a new class of spin excitations which can be excited by ac electric fields. Shortly after, the observation of electromagnons was also reported for multiferroic $YMn_2O_5$ and $TbMn_2O_5$ by Sushkov *et al* [3] and the existence of a hybridized soft magnon mode had been confirmed for $TbMnO_3$ by Senff *et al* [4] using inelastic neutron scattering. Later on, the existence of electromagnons has been reported for $Eu_{1-x}Y_xMnO_3$ [5, 6] in various composition ranges. Theoretically a model of the collective dynamics in simple spiral magnets has been developed by Katsura *et al* [7] who predicted eigenfrequencies of new magnetoelectric excitations, in approximate agreement with the experimental observations. In addition, a renormalization of a phonon mode coupled to the electromagnon has been predicted [7] and confirmed experimentally [8]. Another kind of coupled spin and lattice oscillations in multiferroic manganites was considered in a recent work by Chupis [9] in a polariton-like picture.

The first model calculations of the coupled oscillations in a ferroelectric ferromagnet with collinear spin structure have been published by Baryakhtar and Chupis [10]. These authors included a magnetoelectric term into the equations of motion of spins and lattice, allowing for electric absorption at the spin oscillating frequency and for magnetic absorption at the characteristic ferroelectric frequency. These coupled excitations have been termed 'seignetomagnons'. In a later review of ferroelectromagnets, Smolenskii and Chupis [11]

 

have further developed these ideas and different possibilities to observe these excitations have been discussed. In this work the quanta of coupled oscillations have been called 'ferroelectromagnons'. We would like to stress that these excitations in the first approximation can be seen as renormalized phonons and magnons. Due to the weakness of the corresponding terms no new excitations appear and the effects on the dielectric properties are small. Strong effects may arise at crossing points in the dispersion diagrams of the corresponding excitations only. Due to nonzero wavevector at the crossing point, the effect of such enhancement cannot be observed in static and infrared experiments which are characterized by zero wavevector ($\mathbf{k} = 0$) only.

The fundamentally new point related to the observation of electromagnons is their close relation to incommensurate (IC) magnetic structures. The IC modulation is of fundamental importance for the magnetoelectric interaction itself since it breaks the inversion symmetry which forbids the magnetoelectric effect in simple antiferromagnetic (AFM) phases [12]. In many multiferroic manganites the modulation vectors close to $\mathbf{k}_0 = (0, 0.28, 0)$ have been observed [13–15]. In the antiferromagnetic (AFM) state of the multiferroic manganites the conventional antiferromagnetic resonances (AFMR) are observed as well. Because these are homogeneous oscillations of the magnetization, they are seen, for example, by terahertz spectroscopy as absorption modes, or as $\mathbf{k} = 0$ modes in neutron scattering experiments. In addition to this well-known picture, the spin excitations soften close to the IC modulation vector $\mathbf{k}_0$. This leads to two important new effects: (i) these spin waves interact with electric field due to the ME interaction and (ii) they can be excited by homogeneous electric fields ($\mathbf{k} = 0$) because the wavevectors of the soft mode ($\mathbf{k}_1 = \mathbf{k}_0$) and of the static modulation ($\mathbf{k}_2 = \mathbf{k}_0$) coincide. Therefore, the electromagnons are soft inhomogeneous spin modes which become electrically active due to ME coupling.

The electric nature of electromagnons can be well proven in experiment: as has been explicitly shown in [2], electromagnons can be excited by the electric component of the electromagnetic wave only. They are well separated from antiferromagnetic resonances (AFMR) which are excited by the magnetic ac field of the electromagnetic wave. An example of the simultaneous detection of electromagnons and AFMR in the same spectra is documented in section 4.4. Finally, as will be seen in subsequent sections, electromagnons in multiferroic manganites are observed in incommensurate-antiferromagnetic structures only.

## 2. Experimental details

Most results in this work have been obtained using quasi-optical terahertz BWO spectroscopy [16] in transmittance geometry. Therefore, we briefly present basic ideas of this experimental technique. The beam path of the terahertz spectrometer is shown in figure 1. This spectrometer utilizes linearly polarized monochromatic radiation in the frequency range from 3 to 40 $\mathrm{cm}^{-1}$ which is provided by backward-wave oscillators (BWOs). BWOs are tunable sources of the

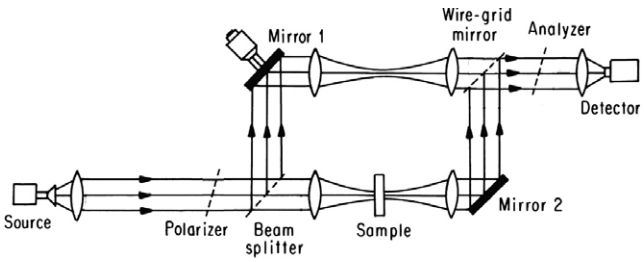


**Figure 1.** Set-up of the quasi-optical terahertz spectrometer.

electromagnetic radiation based on the periodic modulation of the electron beam in a high-vacuum tube [17]. The variation of the output frequency is realized by changing the accelerating voltage in the range of a few kilovolts. The output power of the BWOs is typically 1–100 mW. An opto-acoustic Golay cell or He-cooled bolometer are used as detectors of the radiation. The Mach–Zehnder interferometer arrangement (figure 1) allows us to measure both the intensity and the phase shift of the radiation transmitted through the sample. This technique has been successfully applied to investigate electrodynamic properties of a number of prominent materials [18–20].

Frequency-dependent transmission spectra can be analysed using the Fresnel optical formulae for the transmittance $T = |t|^2$ of a plane parallel sample:

$$t = \frac{(1 - r^2)t_1}{1 - r^2 t_1^2}, \tag{1}$$

where

$$r = \frac{\sqrt{\varepsilon/\mu} - 1}{\sqrt{\varepsilon/\mu} + 1} \qquad \text{and} \qquad t_1 = \exp\{-2\pi \mathrm{i}\sqrt{\varepsilon\mu}d/\lambda\}.$$

Here $r$ is the reflection amplitude at the air–sample interface, $t_1$ is the 'pure' transmission amplitude, $\varepsilon$ and $\mu$ are the complex dielectric permittivity and magnetic permeability of the sample, respectively, $d$ is the sample thickness and $\lambda$ is the radiation wavelength. Equation (1) can be applied for anisotropic crystals as well, provided that the incident radiation is polarized along the principal optical axes.

Equation (1) contains the two unknown material constants, $\varepsilon$ and $\mu$, and cannot be inverted in the general case. Fortunately, at terahertz frequencies the magnetic susceptibility is negligibly small in most cases and $\mu \approx 1$ provides a very good approximation. Nonzero magnetic response can be observed in magnetically ordered samples and in experiments on electron-spin resonance (ESR) [21]. In these cases the magnetic contribution is limited to a narrow frequency range and can be approximated by a Lorentzian. Direct fitting of the spectra using equation (1) and the Lorentzian lineshape allows us to separate electric and magnetic contributions without additional measurements. An example of rigorous extraction of $\varepsilon$ and $\mu$ using two different experimental geometries can be found in [22].

In the infrared frequency range 30 $\mathrm{cm}^{-1} < \nu <$ 6000 $\mathrm{cm}^{-1}$, the complex conductivity has been obtained via the Kramers–Kronig analysis of the reflectivity of a thick sample. In addition, the reflectance for the frequency range

$4\,\mathrm{cm}^{-1} < \nu < 40\,\mathrm{cm}^{-1}$ has been calculated using the complex conductivity data, obtained by the transmittance technique described above. The combination of the results from two experimental techniques [23] substantially expands the low-frequency limit of the available spectrum and the quality of the subsequent Kramers–Kronig transformation.

All samples described in this work have been grown using the floating-zone method with radiation heating. The samples were characterized using x-ray, magnetic and dielectric measurements [24, 25]. The basic properties of our samples agreed well with the results obtained by other groups [1, 26].

## 3. Theory

In this section we present a thermodynamic model for the static electric response of the modulated magnetic structure. An important question which should be answered is why electromagnons are observed both in $GdMnO_3$, in a paraelectric sinusoidal magnetic structure, as well as in $TbMnO_3$, in a ferroelectric with a spiral structure [2]. We consider [8] the ME part of the free energy in terms of the Fourier components of dynamic variables $\mathbf{A}_k$ related to the base antiferromagnetic vector $\mathbf{A}$ of the modulated spin structure [27] (see also [15, 28]):

$$\Phi_{\mathrm{me}} = -\mathrm{i}P_x\Sigma_k a_k^{xz}(\mathbf{A}_k \times \mathbf{A}_k^*)_z - \mathrm{i}P_z\Sigma_k a_k^{zx}(\mathbf{A}_k \times \mathbf{A}_k^*)_x \equiv -\Sigma_k \mathbf{P}\mathbf{E}_{\mathrm{int}}(\mathbf{A}_k), \quad (2)$$

where $\mathbf{P}$ is the electric polarization, ME coefficients $a_k^{xz,zx}$ for the nearest neighbours in the $ab$-lane are determined by $a_k^{xz,zx} = 2Na^{xz,zx}\cos(2\pi kb)\sin(\pi kb)$, where $a^{xz,zx}$ are constants, $N$ is the number of Mn ions and $b$ is the lattice constant. This expression was derived using a crystallographic symmetry ($D_{2h}^{16}$—$Pbnm$ space group) and a modulated spin structure with $\mathbf{k} = (0, k, 0)$. Here we have omitted contributions from other (weak) base vectors $\mathbf{F}_k$, $\mathbf{C}_k$, $\mathbf{G}_k$. In the space representation and continuum limit equation (2) corresponds to $\Phi_{\mathrm{me}} = -a_x P_x(A_x\partial A_y/\partial y - A_y\partial A_x/\partial y) - a_z P_z(A_z\partial A_y/\partial y - A_y\partial A_z/\partial y)$ [2] which for $a_k^{xz} = a_k^{zx}$ is reduced to a Dzyaloshinskii–Moriya type interaction [29–31].

It is clear that, in a homogeneous magnetic state, like in the CA-AFM phase, the ME free energy is zero and no contribution to the dielectric constant, no electromagnons and no spontaneous polarization can exist. To elucidate the ME contribution to the electrical susceptibility in sinusoidal and spiral states we shall consider the total free energy of the system:

$$\Phi(\mathbf{A}_k, \mathbf{P}) = \tfrac{1}{2}N\Sigma_k\big[-J_A(k)\mathbf{A}_k\mathbf{A}_k^* + K_{bc}\mathbf{A}_k^z\mathbf{A}_k^{z*} + K_{ba}\mathbf{A}_k^x\mathbf{A}_k^{x*}\big] - \mathbf{E}\mathbf{P} + \mathbf{P}^2/2\chi_E + \Phi_{\mathrm{me}} - TS(\mathbf{A}_k), \quad (3)$$

where the first three terms correspond to the exchange and anisotropy energy, the forth and fifth terms represent a dielectric contribution in an external electric field $\mathbf{E}$ and the last term is the entropy contribution of the magnetic ions. By minimizing equation (3) with respect to $\mathbf{P}$ it is easy to represent the free energy $\Phi(\mathbf{A}_k)$ as a function of non-equilibrium values of $\mathbf{A}_k$:

$$\Phi(\mathbf{A}_k) = \tfrac{1}{2}N\Sigma_k[-J_A(k)\mathbf{A}_k\mathbf{A}_k^* + K_{bc}\mathbf{A}_k^z\mathbf{A}_k^{z*} + K_{ba}\mathbf{A}_k^x\mathbf{A}_k^{x*}] - \tfrac{1}{2}\chi_E[\mathbf{E} + \mathbf{E}_{\mathrm{int}}(\mathbf{A}_k)]^2 - TS(\mathbf{A}_k). \quad (4)$$

In a sinusoidal spin structure with $\mathbf{A}_k = (0, \mathbf{A}_k^y, 0)$ the electric susceptibility, for example, along the $a(x)$ axis, can be expressed using equations (2)–(4) as

$$\chi_E^x = -\{\partial^2\Phi/\partial E_x^2 + \Sigma_k[\partial^2\Phi/\partial E_x\partial A_k^x(\partial A_k^x/\partial E_x) + \mathrm{c.c.}]\}, \quad (5)$$

where c.c. indicates the complex conjugate and the derivatives $\partial A_k^x/\partial E_x$ are determined by the system of equations

$$\partial^2\Phi/\partial E_x\partial A_k^x + \Sigma_{k'}[\partial^2\Phi/\partial A_k^x\partial A_{k'}^x(\partial A_{k'}^x/\partial E_x) + \mathrm{c.c.}] = 0. \quad (6)$$

Due to the nonlinear entropy term in $\Phi(\mathbf{A}_k)$, i.e.

$$S(\mathbf{A}_k) \approx N(2S+1) - \tfrac{1}{2}\alpha\Sigma_k\mathbf{A}_k\mathbf{A}_k^* - \tfrac{1}{4}\beta\Sigma_{k,k',k''}(\mathbf{A}_k\mathbf{A}_{k'})(\mathbf{A}_{k''}\mathbf{A}_{-k-k'-k''}) + \cdots \quad (7)$$

there exists a coupling of the main harmonic $A_{k0}^y$ corresponding to the maximum of $J_A(k_0)$ with other harmonics $A_k^y(k \neq k_0)$. However, at least near $T_N$ this coupling is weak and we can consider the main harmonic $k_0$ only. In this case

$$\chi_E^x \approx -\partial^2\Phi/\partial E_x^2 + (\partial^2\Phi/\partial E_x\partial A_k^x) \times(\partial^2\Phi/\partial E_x\partial A_k^{x*})/\partial^2\Phi/\partial A_k^x\partial A_k^{x*} \approx \chi_E + (\chi_E a_{k0}^{xz})^2 A_{k0}^y A_{k0}^{y*}/K_{ba}. \quad (8)$$

In the sinusoidal phase no spontaneous polarization can exist since only one $\mathbf{A}_k$ component is nonzero, but the ME contribution to the electric susceptibility arises according to equation (8). It originates from an electric-field-induced rotation of spins in the $ab$ plane, i.e. from the $\mathbf{A}_k^x$ spin components. A similar contribution can also exist along the $c$ axis. Its relative value is determined both by the corresponding magnetoelectric ($a^{xz,zx}$) and magnetic anisotropy ($K_{ba,bc}$) constants.

Finally, in a case with a helical or cycloidally modulated spin structure, for example, $\mathbf{A}_k = (0, \mathbf{A}_k^y, \mathbf{A}_k^z)$, both a spontaneous ferroelectric polarization along the $c$ axis $P_z$ and a finite contribution to the dielectric constant along the $a$ axis $\chi_E^x \approx \chi_E + (\chi_E a_{k0}^{xz})^2 S^2/K_{ba}$, as well as electromagnons, exist.

## 4. Results

In this section we present the results of terahertz experiments on various rare earth multiferroic manganites $RMnO_3$, with R = Tb, Gd, Dy and (Eu:Y). These compounds reveal nonzero magnetoelectric effects and in all compositions the excitations of magnetoelectric nature have been observed at terahertz frequencies. All data are presented for the geometry where the electric field of the radiation is parallel to the $a$ axis. According to existing theoretical models similar excitations can be expected for $e\|c$ as well, but up to now no such effects have been observed experimentally. This apparent contradiction should be clarified in future experiments.

### 4.1. $TbMnO_3$

Among magnetoelectric manganites $TbMnO_3$ is probably one of the most intensively studied by spectroscopic methods. In addition to results from dielectric [1, 32] and optical [2] spectroscopies, the magnetic structure of this material is

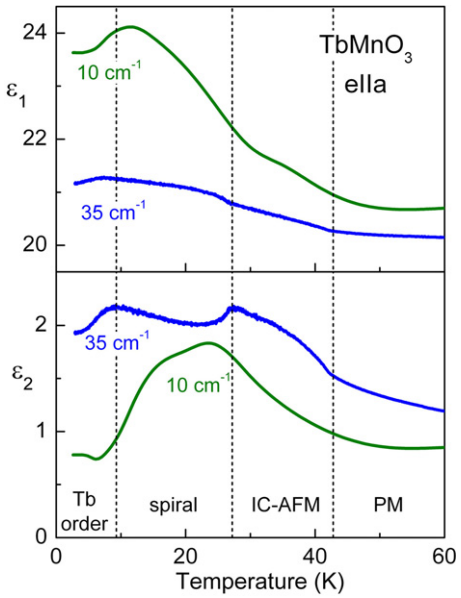


**Figure 2.** Temperature dependence of the terahertz dielectric constant of $TbMnO_3$ along the $a$ axis in zero external magnetic field. Upper panel—real part, lower panel—imaginary part. Dashed lines indicate the temperatures of magnetic phase transitions. PM—paramagnetic, IC-AFM—incommensurate antiferromagnetic (sinusoidal), spiral—spiral (cycloidal) phase, Tb-order—magnetic phase with ordered Tb sublattice.

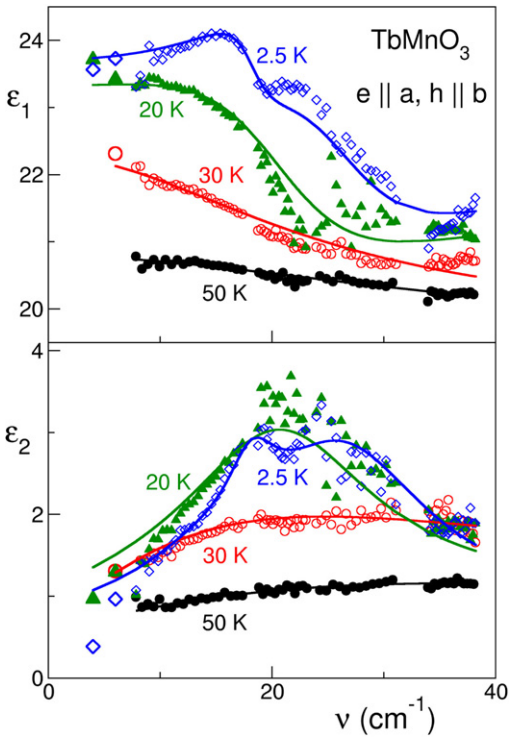


**Figure 3.** Terahertz spectra of $TbMnO_3$ for $e\|a$ at different temperatures. Upper panel—real part, lower panel—imaginary part. Symbols—experiments, lines—fits using the sum of Lorentzians. Large symbols have been obtained from the analysis of the transmittance only. (e) and (h) indicate the ac electric and magnetic fields of the electromagnetic wave, respectively.

well known from neutron scattering experiments [13–15]. In addition, inelastic neutron scattering data are available for $TbMnO_3$ [4] which allow us to compare characteristic frequencies of spin excitations and of electromagnons.

At $T_N = 42$ K $TbMnO_3$ orders antiferromagnetically with the Mn magnetic moments aligned along the $b$ axis with an incommensurate sinusoidal modulation [13–15]. Upon cooling a second transition into a spiral phase occurs at $T_C = 28$ K with a slightly different modulation vector [15]. This low-temperature phase is ferroelectric with spontaneous polarization parallel to the $c$ axis [32]. Finally, a phase transition at about 9 K is attributed to the magnetic ordering of the Tb sublattice. This ordering only weakly affects the ferroelectric and dielectric properties of $TbMnO_3$ [1].

Figure 2 shows the temperature dependence of the dielectric permittivity of $TbMnO_3$ for the ac electric field parallel to the $a$ axis ($e\|a$). All magnetic transitions can be well observed in the dielectric data. This demonstrates already at this stage the coupling between magnetic and electric properties in $TbMnO_3$. The real part of the dielectric permittivity strongly increases with decreasing temperature which reflects the growth of the magnetoelectric contribution. The initial increase of the imaginary part on cooling is reversed below $T_C = 28$ K. As can be seen in the spectra below, this reflects the narrowing of the electromagnon. Below $T = 10$ K distinct structure is observed both in $\varepsilon_1$ and in $\varepsilon_2$. This points towards an additional excitation with the energy around 10 $cm^{-1}$ and with a temperature-dependent characteristic frequency.

Figure 3 shows the terahertz spectra of $TbMnO_3$ for an ac electric field parallel to the $a$ axis ($e\|a$). We recall that this is the only axis with substantial absorption at terahertz frequencies. Both other directions are nearly transparent to terahertz radiation. For decreasing temperatures an overdamped excitation starts to grow in the spectra for $e\|a$. In the real part of the dielectric permittivity this excitation is seen as a broad step-like increase towards low frequencies which corresponds to a maximum in the imaginary part. This broad feature can be identified as an electromagnon. Especially in the spiral phase below 28 K the electromagnon narrows and becomes a well-defined excitation close to 23 $cm^{-1}$. The spectral weight of the electromagnon continues to increase on cooling. In the spiral phase the electromagnon splits into two modes at 18 and at 24 $cm^{-1}$. This splitting is well documented at $T = 2.5$ K because both components of the electromagnon narrow at low temperatures. Comparing this result with the low-temperature feature observed in figure 2, we conclude that the mode at 18 $cm^{-1}$ originally appears at zero frequencies and is probably the same as the low-frequency mode observed close to 9 $cm^{-1}$ in inelastic neutron scattering [4]. These experiments revealed two basic magnetic excitations in $TbMnO_3$ in the spiral AFM phase at $T = 17$ K, at 9 and at 20 $cm^{-1}$. The latter excitation corresponds well to the electromagnon seen in the terahertz spectra at 23 $cm^{-1}$.

### 4.2. $GdMnO_3$

The high-temperature paramagnetic phase in $GdMnO_3$ is followed by an incommensurate (IC) AFM phase below $T_N =$

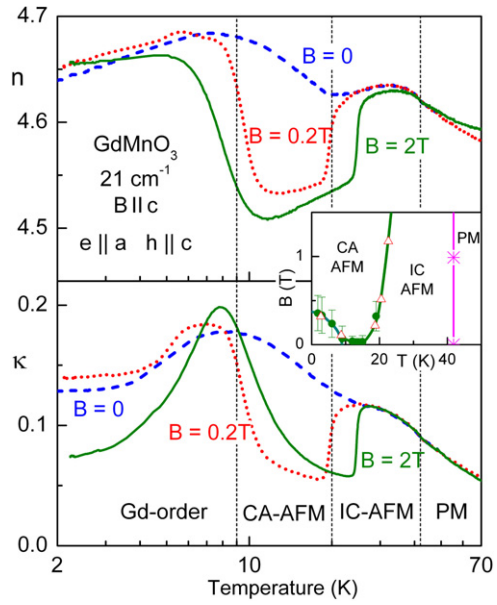


**Figure 4.** Temperature dependence of the terahertz dielectric properties of $GdMnO_3$ along the $a$ axis with different external magnetic fields applied parallel to the $c$ axis. The data are obtained on heating from the initial zero-field-cooled state. The results are presented in the form of the complex refraction index $n + i\kappa = \sqrt{\varepsilon\mu}$ due to a mixing of magnetic and electric contributions below 12 K. Above this temperature the magnetic contribution can be neglected ($\mu \approx 1$). The vertical dashed lines mark the temperature of the magnetic phase transitions: PM—paramagnetic, AFM—antiferromagnetic, IC—incommensurate (sinusoidally modulated), CA—canted, Gd-order—magnetic phase with ordered Gd sublattice. The inset shows the $(B, T)$ phase diagram obtained from dielectric and magnetic measurements.

42 K. This phase is characterized by a sinusoidally modulated spin structure of the manganese spins, with the Gd spins still remaining paramagnetic [24]. In low fields ($B < 0.1$ T) and under zero-field-cooling conditions the IC structure remains the stable phase down to 8 K and is followed by a complex canted ferrimagnetic structure of Gd and Mn spins. In finite magnetic fields along the $c$ axis ($B > 0.1$ T) the IC-AFM phase is transformed to a canted antiferromagnetic (CA-AFM) state with the ferromagnetic $c$-axis components of the manganese and gadolinium spins oriented antiparallel. Details of this structure are unknown, but it is clear that in this phase the Gd spins participate in the magnetic order. Between 8 K $< T <$ 17 K this spin arrangement strongly competes with the IC-AFM phase and, depending on the magnetic history, the canted antiferromagnet can be stabilized even in zero external magnetic fields. A detailed phase diagram, obtained using dielectric and magnetic data [2], is shown as the inset in figure 4. Contrary to $TbMnO_3$, without an external magnetic field $GdMnO_3$ remains in the paraelectric state in all low-temperature phases. Only in the external magnetic fields along the $b$ axis can the ferroelectricity be induced [1] which might be due to formation of the spiral magnetic phase.

Figure 4 shows the terahertz dielectric properties of $GdMnO_3$ as a function of temperature. These results are shown in a representation $n + i\kappa$, where $n$ is the refraction index and $\kappa$ is the absorption coefficient. This representation has been chosen because of the mixing of the electric and magnetic contribution below 12 K and in the geometry $e\|a, h\|c$. In this case the experimental transmittance and phase shift must be described both by the dielectric permittivity $\varepsilon_a = \varepsilon_1 + i\varepsilon_2$ and the magnetic permeability $\mu_c = \mu_1 + i\mu_2$. An unambiguous separation of both properties is not possible. In a good and representative approximation the results can be plotted in the form $(n+i\kappa)^2 = \varepsilon\mu$. Above $T = 12$ K the dynamic properties are purely dielectric ($\mu = 1$) and the complex dielectric function can be easily calculated via $(n + i\kappa)^2 = \varepsilon_1 + i\varepsilon_2$, which in this case may be simplified to $n^2 \approx \varepsilon_1$ and $2n\kappa = \varepsilon_2$.

At temperatures between 9 and 20 K the data in figure 4 correspond to the CA-AFM phase, which agrees well with the experiments at low frequencies [1, 24]. The only difference to the low-frequency properties is the extreme weakness of the CA–IC transition in the THz data in zero magnetic field. In contrast to the static dielectric properties, in figure 4 only small changes are observed at $T_{CA} \approx 20$ K with $B = 0$. The observed discrepancy between THz and kHz data can be accounted for using different sensitivities of low- and high-frequency spectroscopy to these small changes and to a frequency dependence of the corresponding contributions. Strong field-dependent changes, observed in figure 4 close to $T = 9$ K, are due to the influence of the AFMR mode in $GdMnO_3$ around 21 $cm^{-1}$. Because of a temperature dependence of the mode frequency, temperature-dependent experiments at a fixed frequency are sensitive to this mode. It is important to note that the present AFMR mode is excited by the magnetic ac component of the radiation, which is parallel to the $c$ axis in this experimental configuration. Therefore [33], this mode corresponds to the so-called quasi-antiferromagnetic branch of the AFMR mode.

Figure 5 shows terahertz spectra of $GdMnO_3$ for the electric field parallel to the $a$ axis and at different temperatures. Compared to the results shown in figure 4 these data have been obtained with the ac magnetic field parallel to the $b$ axis ($e\|a, h\|b$, $ab$-plane sample). Therefore, the antiferromagnetic resonance at 21 $cm^{-1}$ is not excited in this geometry and the pure dielectric response can be presented.

Similar to the data in $TbMnO_3$, a broad relaxation-like contribution can be observed already in the paramagnetic phase, which is probably due to magnetoelectric fluctuations. We attribute this broad contribution to an over-damped electromagnon. The electromagnon remains over-damped in the sinusoidal phase and grows for decreasing temperature. Substantial narrowing of this excitation is observed below 20 K. As discussed above, the CA-AFM phase can be reached only in external magnetic fields. Because the data in figure 5 have been obtained in zero magnetic field, the low-temperature data still correspond to the incommensurate metastable phase.

The dielectric strength of the electromagnon decreases below the temperature of the Gd ordering. A similar tendency has been observed in $TbMnO_3$, too. In $GdMnO_3$ the intensity of the electromagnon at 24 $cm^{-1}$ decreases and instead an additional narrow peak appears at 15 $cm^{-1}$. This peak is most clearly seen in $T = 2.5$ K spectra but can be detected at $T = 5$ K as well. By analogy to $TbMnO_3$ this splitting reflects the fine structure of the electromagnon. However, an important

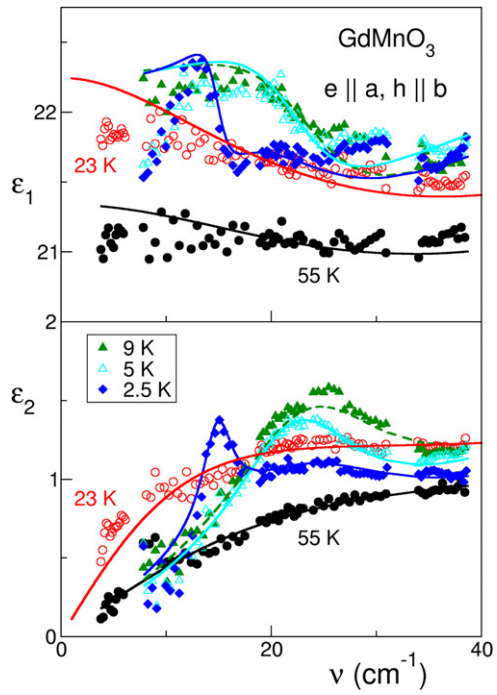


**Figure 5.** Terahertz dielectric spectra of $GdMnO_3$ along the *a* axis. Upper panel—real part, lower panel—imaginary part. Symbols—experiments, lines—fits using the sum of Lorentzians.

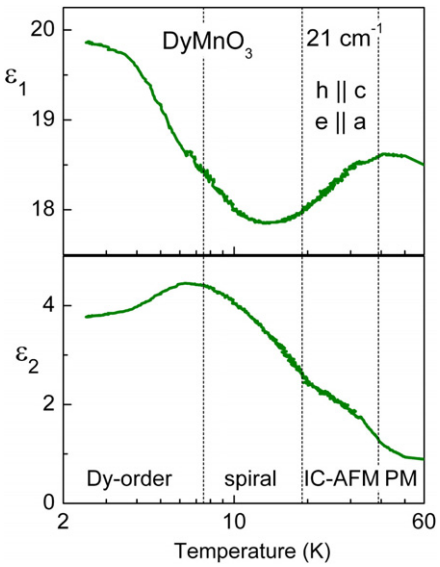


**Figure 6.** Temperature dependence of the terahertz dielectric permittivity of $DyMnO_3$ along the *a* axis and in zero external magnetic field. Upper panel—real part, lower panel—imaginary part. Dashed lines indicate the temperatures of the magnetic phase transitions. PM—paramagnetic, IC-AFM—incommensurate antiferromagnetic (sinusoidal), Dy-order—magnetic phase with ordered Dy sublattice.

difference compared to $TbMnO_3$ is the absence of the spiral structure in $GdMnO_3$ in zero magnetic fields according to magnetization data. From dielectric results we can nevertheless suggest the appearance of a spiral structure in $GdMnO_3$, which is realized probably in a dynamic way. Another support for this suggestion is the narrowing of the electromagnon below 23 K, which in other multiferroic manganites is observed only in the spiral phase. Further experiments are needed to clarify this point.

### *4.3. $DyMnO_3$*

$DyMnO_3$ is very similar to $TbMnO_3$ concerning magnetic, structural and dielectric properties. $DyMnO_3$ shows an incommensurate (probably sinusoidally modulated) antiferromagnetic structure below $T_N \approx 39$ K. At lower temperatures a second phase transition into a ferroelectric phase takes place at $T_C \approx 18$ K. By analogy to $TbMnO_3$ and other rare earth manganite multiferroics this phase is probably a spiral antiferromagnet. An indirect support of this statement is the appearance of a static ferroelectric polarization which occurs in spiral structures due to a breaking of the spatial and time inversion symmetry. Finally, at $T \sim 7.5$ K another magnetic transition is observed which is characterized by the ordering of the Dy sublattice.

In contrast to $TbMnO_3$ and $GdMnO_3$ the magnetic phases of $DyMnO_3$ are robust in external magnetic fields along the *c* axis. This robustness has been proven experimentally up to fields of $B_c = 9$ T [1]. Magnetic phase transitions in $DyMnO_3$ are indicated in figure 6 by dashed lines. Figure 6 shows the temperature dependence of the dielectric permittivity of $DyMnO_3$ at a frequency of 21 $cm^{-1}$. Only weak anomalies in dielectric properties can be observed at the magnetic phase transitions. This is partly due to the relatively high frequency of this experiment compared to the characteristic frequency of the electromagnon in $DyMnO_3$ (about 15 $cm^{-1}$).

Due to the stability of magnetic structure the magnetoelectric contribution in this compound cannot be suppressed by external magnetic fields. Another characteristic difference compared to $TbMnO_3$ is the substantially lower frequency of the electromagnon. This is demonstrated in figure 7 which shows terahertz spectra of $DyMnO_3$ for $e \| a$. A significant magnetoelectric contribution (electromagnon) appears in $DyMnO_3$ below $T_N = 39$ K and at low frequencies. Below the transition to the spiral phase this contribution narrows showing an eigenfrequency around 15 $cm^{-1}$. Similar to the behaviour in $TbMnO_3$ and $GdMnO_3$ the dielectric strength of the electromagnon in $DyMnO_3$ decreases below the Dy ordering. In contrast to $TbMnO_3$ and $GdMnO_3$ in these spectra we do not observe additional excitations at low frequencies. However, preliminary results in the frequency range below 8 $cm^{-1}$ point to the existence of such an additional mode around 5 $cm^{-1}$.

Very recently, Kida *et al* [34] presented terahertz spectra in $DyMnO_3$ using time domain spectroscopy. These results basically agree with the data shown above and revealed a strong excitation around 16 $cm^{-1}$ and a second weaker mode around 44 $cm^{-1}$. Both excitations have been demonstrated to interact with the electric component of the radiation.

### *4.4. $Eu_{1-x}Y_xMnO_3$*

A common property of the above-discussed Tb, Gd and Dy manganites is the existence of two competing magnetic

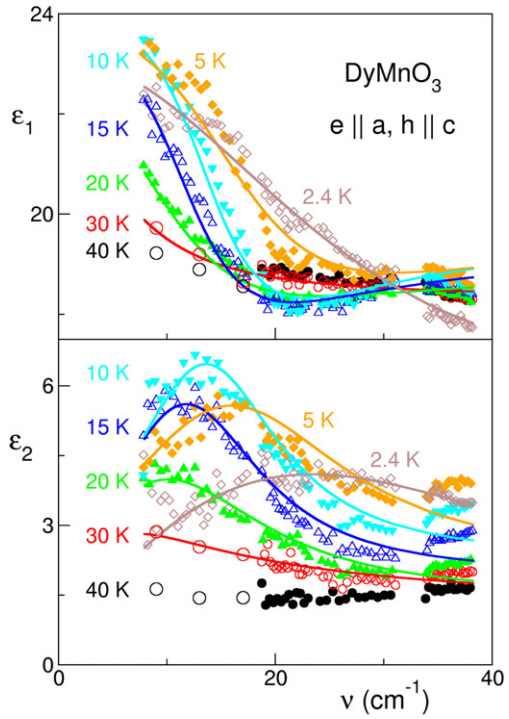


**Figure 7.** Terahertz dielectric spectra of $DyMnO_3$ along the $a$ axis. Upper panel—real part, lower panel—imaginary part. Symbols—experiments, lines—Lorentzian fits. Large symbols have been obtained from the analysis of the transmittance only.

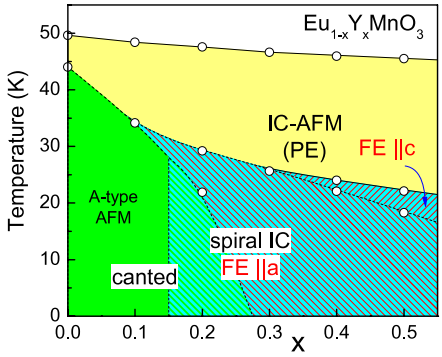


**Figure 8.** $(T, x)$ phase diagram of $Eu_{1-x}Y_xMnO_3$ reproduced from [6]. The notation of magnetic phases is given on the basis of magnetization data. AFM—antiferromagnetic phase, IC—incommensurate, PE—paraelectric, FE—ferroelectric. The exact magnetic structure of different phases is still unknown and is indicated by analogy to other perovskite multiferroics.

sublattices of Mn and of the rare earth. At present the role of the rare earth subsystem in the magnetoelectric interaction is not quite clear. In order to separate the role of the rare earth from the magnetoelectric effects in manganites it is expedient to repeat the experiments on manganites without rare earth magnetism. Such a system is provided by $Eu_{1-x}Y_xMnO_3$, where a further tuning parameter is achieved through doping by yttrium.

Detailed investigation of the magnetic and dielectric properties of $Eu_{1-x}Y_xMnO_3$ have been published in [25]. From these data a magnetic and electric phase diagram has been constructed which is represented in figure 8. In the doping range $0 \leqslant x \leqslant 0.5$ $Eu_{1-x}Y_xMnO_3$ orders antiferromagnetically between 45 and 50 K, only slightly depending upon the yttrium content. The antiferromagnetic order is incommensurate and probably sinusoidally modulated similar to other rare earth multiferroics. On further cooling another magnetic transition takes place. Depending on the doping range, this low-temperature phase is either canted antiferromagnetic for $x < 0.2$ or spiral and ferroelectric for $x \geqslant 0.2$. For $x \approx 0.2$ the magnetic phase probably is a spiral with a conical distortion.

The most important point concerning the results in $Eu_{1-x}Y_xMnO_3$ is that magnetoelectric effects and electromagnons are observed in the full doping range $0 \leqslant x \leqslant 0.5$. This excludes the influence of the rare earth magnetism as a basic mechanism for the magnetoelectric effects in rare earth multiferroic manganites.

Detailed terahertz properties of $Eu_{1-x}Y_xMnO_3$ have been published in [6]. Here we reproduce two examples of magnetoelectric excitations in these compounds and discuss the basic differences as a function of doping. From the point of view of the magnetoelectric effect and the observation of electromagnons, the phase diagram in figure 8 can be divided into four regimes.

(i) In the low-doping range $0 \leqslant x \leqslant 0.1$ in the IC-AFM phase weak ME effects are observed and the electromagnons are over-damped and not well defined. The IC-AFM phase in this region is followed by the canted CA-AFM phase which shows no magnetoelectric effect.

(ii) At low temperatures the phase around $x = 0.2$ is characterized both by a spiral IC-AFM structure (FE$\|a$) and by the existence of a weak ferromagnetism. In this region the electromagnons are clearly observed in the spectra and can be suppressed by external magnetic fields, which leads to strong magnetic field dependence of the dielectric permittivity.

(iii) For $x \approx 0.3$ the electromagnons are strong in the ferroelectric phase at low temperatures but they are not sensitive to external magnetic fields up to 7 T.

(iv) The region $0.4 \leqslant x \leqslant 0.5$ is closely similar to $x \approx 0.3$, but here the dielectric permittivity is weakly dependent upon external magnetic fields in a narrow temperature range, where ferroelectric phases with electric polarization parallel to the $a$- and $c$-axes compete.

As an example of magnetoelectric excitations at low doping, figure 9 shows the terahertz spectra of $Eu_{0.9}Y_{0.1}MnO_3$. Here the data at 40 and 20 K are representative of the properties in the IC-AFM and CA-AFM phases, respectively. Compared to the canted phase, additional absorption of magnetoelectric origin is clearly seen in the spectra of the IC phase. As a typical feature of the sinusoidal phase, the electromagnon is seen as a broad Debye-like relaxation only. Typical frequency of this excitation can be estimated as 10 $cm^{-1}$. The magnetoelectric contribution to the dielectric permittivity in $Eu_{0.9}Y_{0.1}MnO_3$ can be suppressed in external magnetic fields which favours the canted magnetic phase. An example of such behaviour is shown in the inset of figure 9.

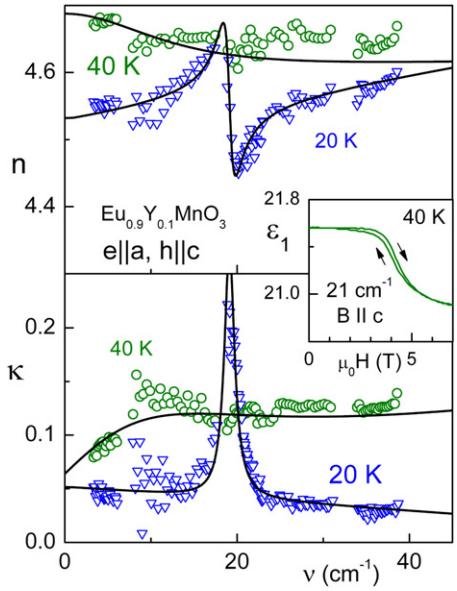


**Figure 9.** Terahertz spectra of $Eu_{0.9}Y_{0.1}MnO_3$ in the incommensurate (40 K) and canted (20 K) antiferromagnetic phases [6]. Upper panel—refractive index, lower panel—absorption coefficient. The narrow mode at $\nu \simeq 19$ cm$^{-1}$ represents the antiferromagnetic resonance ($h \| c$). The broad additional absorption for $T = 40$ K is of magnetoelectric origin. Symbols represent the experimental data, lines show the fits using the sum of Lorentzians and a Debye relaxator. The inset shows the magnetic field dependence of the dielectric constant on the border between IC and CA phases.

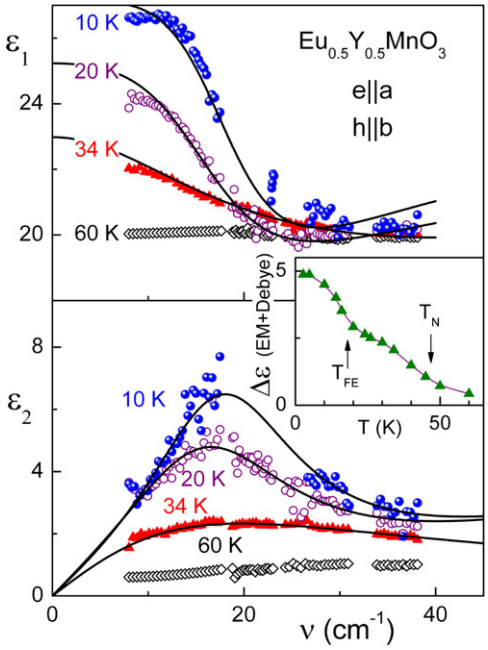


**Figure 10.** Spectra of the dielectric permittivity of $Eu_{0.5}Y_{0.5}MnO_3$ for $e \| a$. Upper panel—real part, lower panel—imaginary part. Symbols—experiment, lines—Lorentzian fits. Inset shows the dielectric contribution of the electromagnon and the Debye relaxator.

With increasing doping, the electromagnons in $Eu_{1-x}Y_xMnO_3$ narrow and their spectral weight increases. A typical behaviour seen in the heavily doped composition $Eu_{0.5}Y_{0.5}MnO_3$ is represented in figure 10. As demonstrated in the inset in figure 10, the magnetoelectric contribution can be observed already in the paramagnetic state and increases on cooling in the ordered magnetic phases. In the spiral phase the electromagnon is well defined and reveals a characteristic frequency of about 18 cm$^{-1}$.

## 5. Discussion

Comparing the spectra of different multiferroic manganites presented above, some general conclusions about the electromagnons can be drawn. In the collinear incommensurate and paramagnetic phase a broad magnetoelectric contribution exists in the terahertz spectra of all samples. This broad contribution seems to result from the same mechanisms as the electromagnon response. It can be described using a Debye-like relaxation and is observed already in the paramagnetic phase, possibly due to magnon-like fluctuations. In addition to the broad contribution a well-defined electromagnon starts to grow in the spiral FE state on the costs of the Debye relaxator. On cooling, all samples show an increase of the magnetoelectric strength, which can be directly observed experimentally as an increase of the low-frequency dielectric constant. Except for $Eu_{1-x}Y_xMnO_3$ additional modes arise at low temperatures and reflect the fine structure of electromagnons. Schematically, the

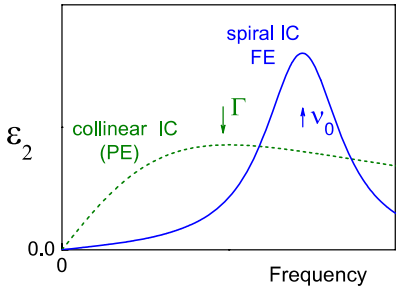


**Figure 11.** Schematic representation of the terahertz spectra of magnetoelectric manganites. Paramagnetic (PM) phase shows no magnetoelectric contribution; the collinear incommensurate-antiferromagnetic (IC-AFM) and paraelectric (PE) phase reveals a broad Debye-like response; in a spiral (cycloidal) ferroelectric (IC-FE) phase well-defined electromagnons are observed. Arrows indicate the damping of the relaxator $\Gamma$ and the eigenfrequency of the electromagnon $\nu_0$.

evolution of the electromagnons with temperature is given in figure 11.

The magnetoelectric interaction leads not only to the appearance of electromagnons in multiferroic manganites, but also to a static electric polarization in the spiral phase. It is therefore clear that the appearance of the electromagnons in the spectra must correspond to lattice distortions.

Experimentally, this effect can be observed as a coupling between the electromagnons and the phonons and has been proven in $GdMnO_3$ [8]. The basic result of this experiment is shown in figure 12. The combination of the terahertz and infrared spectroscopies allowed simultaneous estimation of the dielectric contributions of the electromagnon and of

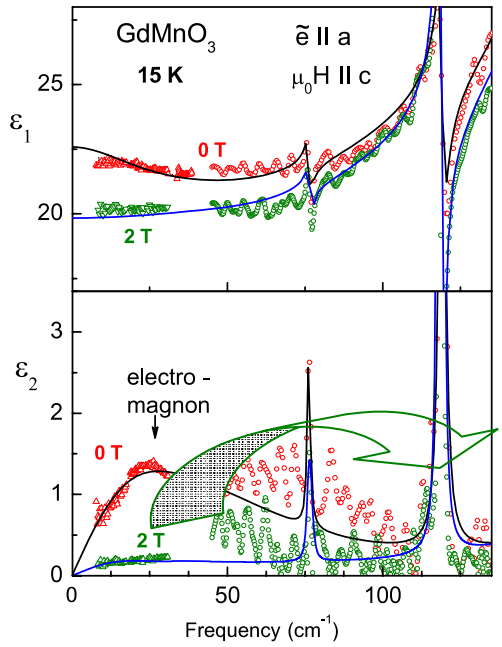


**Figure 12.** Spectra of the *a*-axis dielectric permittivity of $GdMnO_3$ in the frequency range between the electromagnon at ∼25 $cm^{-1}$ and the phonon at 119 $cm^{-1}$ at $B = 0$ T (IC-AFM state) and $B = 2$ T (CA-AFM state). Upper panel: real part of the dielectric permittivity, lower panel: imaginary part. Symbols—experiment (terahertz and infrared spectroscopies). Solid lines correspond to the sum of Lorentzians to account for electromagnon and phonons. The thick arrow indicates the transfer of the spectral weight from the electromagnon to the phonons.

the phonons on switching the magnetic state from the IC-AFM (electromagnon exists) to the CA-AFM (electromagnon is suppressed). As can be most clearly seen in the lower panel of figure 12, on suppression of the electromagnon the amplitude of the lowest phonon for this geometry ($e \| a$) increases. Detailed analysis, as given in [8], revealed that both processes indeed take place simultaneously at a critical field close to 0.2 T. Strictly speaking, the property which must be conserved in this case is the full spectral weight. The spectral weight corresponds to the total number of electrons in the sample and is defined as

$$S = \frac{2}{\pi \varepsilon_0} \int_0^\infty \sigma_1(\omega)\, \mathrm{d}\omega,$$

where $\sigma_1 = \varepsilon_0 \varepsilon_2 \omega$ is the real part of the complex conductivity and $\omega = 2\pi\nu$ is the angular frequency. For a Lorentzian, this definition may be simplified as $S = \Delta\varepsilon\omega_0^2$, where $\omega_0$ is the eigenfrequency. From the fits of the spectra in figure 12 the increase of the phonon spectral weight has been estimated as $\Delta S_{\mathrm{ph}} = 1.7 \times 10^3$ $cm^{-2}$ and the decrease of the electromagnon spectral weight as $\Delta S_{\mathrm{em}} = 2.5 \times 10^3$ $cm^{-2}$. (We note that in [8] a substantially smaller value of the $\Delta S_{\mathrm{em}}$ has been given because, instead of eigenfrequency, the position of the absorption maximum has been utilized to calculate the spectral weight.) We can conclude that at the phase transition to the canted magnetic phase the spectral weight is roughly transferred from the electromagnon to the lowest phonon. As $\Delta S_{\mathrm{em}}$ is slightly larger than $\Delta S_{\mathrm{ph}}$, higher frequency excitations probably gain the remaining weight. However, this transfer could not be observed in [8] within the experimental accuracy.

The coupling between electromagnons and phonons agrees well with the recent model calculations for spiral magnetic structures [7]. For the dynamic properties the main result of these calculations is the occurrence of two modes, one of which is derived from the phonon mode with a frequency close to the eigenfrequency of the uncoupled phonon, and one originating from the spin wave with a frequency proportional to $\sqrt{SJD}$, where $S$ is the spin value, $J$ is the exchange coupling and $D$ is the anisotropy. Using realistic parameters the electromagnon frequency of $\nu_{\mathrm{p}} \sim 10$ $cm^{-1}$ has been calculated [7] which is close to the experimental observation.

## 6. Conclusions

In this work we reviewed the spectra of electromagnons in rare earth multiferroic manganites $RMnO_3$ obtained using terahertz spectroscopy. From the analysis we conclude that, from the spectroscopic point of view, electromagnons represent the mechanism of the magnetoelectric effect in multiferroic manganites.

In all compositions with magnetoelectric interaction the electromagnons could be observed in the frequency range $10\ cm^{-1} < \nu < 30\ cm^{-1}$. The existence of electromagnons does not depend upon the rare earth magnetic sublattice. In some compositions and at low temperatures additional structure in the electromagnon spectrum has been observed.

From the comparative analysis of all data some general behaviour of the magnetoelectric excitations can be drawn. In the collinear IC-AFM phase the electromagnons are overdamped and not well defined. They are seen as broad absorption only in the IC-AFM phase and partly even in the paramagnetic phase. Below the transition to the spiral state the electromagnons narrow and can be clearly seen in the spectra. Similar energies of electromagnons in rare earth multiferroic manganites are probably due to similar strength of the magnetic interactions in all presented compounds.

## References

[1] Kimura T, Lawes G, Goto T, Tokura Y and Ramirez A P 2005 *Phys. Rev.* B **71** 224425
[2] Pimenov A, Mukhin A A, Ivanov V Y, Travkin V D, Balbashov A M and Loidl A 2006 *Nat. Phys.* **2** 97
[3] Sushkov A B, Aguilar R V, Cheong S W and Drew H D 2007 *Phys. Rev. Lett.* **98** 027202
[4] Senff D, Link P, Hradil K, Hiess A, Regnault L P, Sidis Y, Aliouane N, Argyriou D N and Braden M 2007 *Phys. Rev. Lett.* **98** 137206
[5] Aguilar R V, Sushkov A B, Zhang C L, Choi Y J, Cheong S W and Drew H D 2007 *Phys. Rev.* B **76** 060404(R)
[6] Pimenov A, Loidl A, Mukhin A A, Travkin V D, Ivanov V Yu and Balbashov A M 2008 *Phys. Rev.* B **77** 014438
[7] Katsura H, Balatsky A V and Nagaosa N 2007 *Phys. Rev. Lett.* **98** 027203
[8] Pimenov A, Rudolf T, Mayr F, Loidl A, Mukhin A A and Balbashov A M 2006 *Phys. Rev.* B **74** 100403(R)
[9] Chupis I E 2007 *Low Temp. Phys.* **33** 952
[10] Baryakhtar V G and Chupis I E 1970 *Sov. Phys.—Solid State* **11** 2628

[11] Smolenskii G A and Chupis I E 1982 *Sov. Phys.—Usp.* **25** 485
[12] Cheong S W and Mostovoy M 2007 *Nat. Mater.* **6** 13
[13] Quezel S, Tcheou F, Rossat-Mignod J, Quezel G and Roudaut E 1977 *Physica* B+C **86** 916
[14] Kajimoto R, Yoshizawa H, Shintani H, Kimura T and Tokura Y 2004 *Phys. Rev.* B **70** 012401
[15] Kenzelmann M, Harris A B, Jonas S, Broholm C, Schefer J, Kim S B, Zhang C L, Cheong S W, Vajk O P and Lynn J W 2005 *Phys. Rev. Lett.* **95** 087206
[16] Volkov A A, Goncharov Yu G, Kozlov G V, Lebedev S P and Prokhorov A M 1985 *Infrared Phys.* **25** 369
[17] Kozlov G V and Volkov A A 1998 Coherent source submillimeter wave spectroscopy *Millimeter and Submillimeter Wave Spectroscopy of Solids* ed G Grüner (Berlin: Springer) p 51
[18] Mukhin A A, Ivanov V Y, Travkin V D, Pimenov A, Loidl A and Balbashov A M 2000 *Europhys. Lett.* **49** 514
[19] Pimenov A, Tachos S, Rudolf T, Loidl A, Schrupp D, Sing M, Claessen R and Brabers V A M 2005 *Phys. Rev.* B **72** 035131
[20] Pronin A V, Dressel M, Pimenov A, Loidl A, Roshchin I V and Greene L H 1998 *Phys. Rev.* B **57** 14416
[21] Ivannikov D, Biberacher M, Krug von Nidda H-A, Pimenov A, Loidl A, Mukhin A A and Balbashov A M 2002 *Phys. Rev.* B **65** 214422
[22] Pimenov A, Loidl A, Gehrke K, Moshnyaga V and Samwer K 2007 *Phys. Rev. Lett.* **98** 197401
[23] Pimenov A, Loidl A and Krasnosvobodtsev S I 2002 *Phys. Rev.* B **65** 172502
[24] Hemberger J, Lobina S, Krug von Nidda H-A, Tristan N, Ivanov V Yu, Mukhin A A, Balbashov A M and Loidl A 2004 *Phys. Rev.* B **70** 024414
[25] Hemberger J, Schrettle F, Pimenov A, Lunkenheimer P, Ivanov V Y, Mukhin A A, Balbashov A M and Loidl A 2007 *Phys. Rev.* B **75** 035118
[26] Goto T, Kimura T, Lawes G, Ramirez A P and Tokura Y 2004 *Phys. Rev. Lett.* **92** 257201
[27] Bertaut E F 1963 *Magnetism* vol III, ed T Rado and H Suhl (New York: Academic) p 149
[28] Lawes G, Harris A B, Kimura T, Rogado N, Cava R J, Aharony A, Entin-Wohlman O, Yildirim T, Kenzelmann M, Broholm C and Ramirez A P 2005 *Phys. Rev. Lett.* **95** 087205
[29] Katsura H, Nagaosa N and Balatsky A V 2005 *Phys. Rev. Lett.* **95** 057205
[30] Mostovoy M 2006 *Phys. Rev. Lett.* **96** 067601
[31] Sergienko I A and Dagotto E 2006 *Phys. Rev.* B **73** 094434
[32] Kimura T, Goto T, Shintani H, Ishizaka K, Arima T and Tokura Y 2003 *Nature* **426** 55
[33] Mukhin A A, Biberacher M, Pimenov A and Loidl A 2004 *J. Magn. Reson.* **170** 8
[34] Kida N, Ikebe Y, Takahashi Y, He J P, Kaneko Y, Yamasaki Y, Shimano R, Arima T and Tokura Y 2007 *Preprint* 0711.2733v1